J. Fluid Mech. (1991), *vol.* 233, *pp.* 389–404
Printed in Great Britain

Laboratory measurements of modulation of short-wave slopes by long surface waves

By SARAH J. MILLER[1], OMAR H. SHEMDIN[1] AND MICHAEL S. LONGUET-HIGGINS[2]

[1] Ocean Research and Engineering, 255 South Marengo Avenue, Pasadena, CA 91101, USA

[2] Institute for Nonlinear Science, University of California San Diego, La Jolla, CA 92093-0402, USA

(Received 17 December 1990 and in revised form 28 May 1991)

Hydrodynamic modulation of wind waves by long surface waves in a wave tank is investigated, at wind speeds ranging from 1.5 to 10 m s^{-1}. The results are compared with the linear, non-dissipative, theory of Longuet-Higgins & Stewart (1960), which describes the modulation of a group of short gravity waves due to straining of the surface by currents produced by the orbital motions of the long wave, and work done against the radiation stresses of the short waves. In most cases the theory is in good agreement with the experimental results when the short waves are not too steep, and the rate of growth due to the wind is relatively small. At the higher wind speeds, the effects of wind-wave growth, dissipation and wave–wave interactions are dominant.

1. Introduction

The modulation of radar reflections from surface water waves depends, at least in part, on hydrodynamic modulation. A nonlinear theory for the propagation of short waves on longer gravity waves has been available for some time (Longuet-Higgins & Stewart 1960; Longuet-Higgins 1987). However, there have been relatively few *direct* measurements of hydrodynamic modulation of wind waves by longer surface waves. Reece (1978) studied the modulation of the frequency spectrum of short surface waves, as indicated by radar backscatter, in a wave tank and had to contend with the added complications of large, variable Doppler effects. Wright *et al.* (1980) used radar to investigate the variation of microwave power scattered by short ocean waves on long surface waves. Here, hydrodynamic effects represent just one contribution to the resultant backscatter modulation. Rather more experimental investigations have been focused on short-wave/internal-wave interactions (for example, Lewis, Lake & Ko 1974; Hughes & Grant 1978; Kwoh, Lake & Rungaldier 1988), where the modulation tends to be large.

Direct measurements of modulation by surface waves are needed, made under the simplest possible conditions. In the laboratory, wave parameters can be controlled and stable environmental conditions can be reproduced. Also, long time series can be generated, and reliable statistics of short-wave quantities can be obtained by averaging over equal phases of the long wave, a technique which is only applicable in the laboratory. In the following we present the results of an experiment in which wind waves were generated in a wind-wave tank using a range of wind speeds from 1.5 to 10 m s^{-1}. These were modulated by a mechanically generated (6 m long) surface wave. One unexpected finding is that the higher harmonics in the

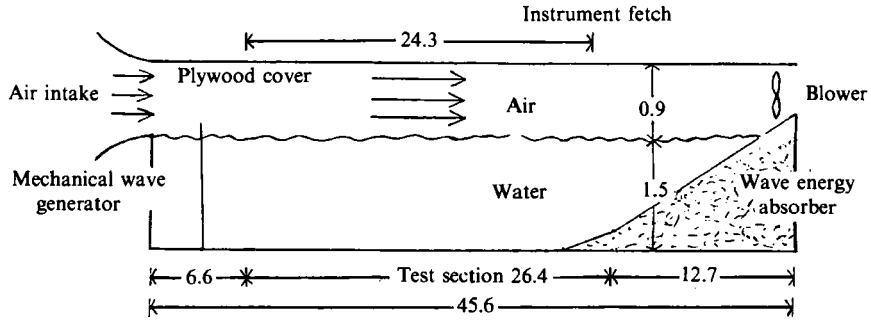

(*a*) Side view

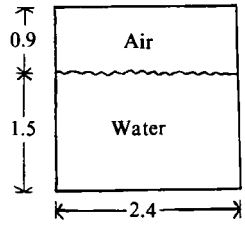

(*b*) End view

FIGURE 1. Schematic diagram of SIO wind and wave facility (reproduced from Miller & Shemdin 1991). Dimensions in m.

mechanically generated wave, though invisible to the naked eye, play an important role in modulating the steepness of the wind-generated waves.

The same data set was the subject of a previous investigation by two of us (Miller & Shemdin 1991), but that work had a different emphasis from that presented here, being concerned with modulation in a *spectral* sense. The change in the level of the encountered frequency spectrum of short-wave slopes, due to hydrodynamic modulation and Doppler shifting caused by the long surface wave, was considered for spectral components in the frequency band 10 to 20 Hz. The observed modulation was compared with the predictions of a linearized solution of the radiative transfer equation.

The present paper considers modulation of the total mean-square slope of short waves. The details of the experimental configuration are described in §2. In §3 the variation of the mean-square slopes of the short waves over the long-wave profile is examined. The results are compared with the linear, non-dissipative theory of Longuet-Higgins & Stewart (1960) in §4. A discussion follows in §5.

2. Experimental set-up

The experimental conditions are described in Miller & Shemdin (1991) and are summarized here for completeness. The experiment was carried out using a wind-wave facility at the Scripps Institution of Oceanography. A diagram of the wind-wave tank is shown in figure 1. The facility test section is 26.4 m long and 2.4 m wide. The water depth was set at 1.5 m during the test. Wind waves were generated using a blower which was operated to obtain wind speeds in the range 1.5 to 10 m s^{-1}. Low-frequency mechanical waves could be generated using a paddle located at the upwind

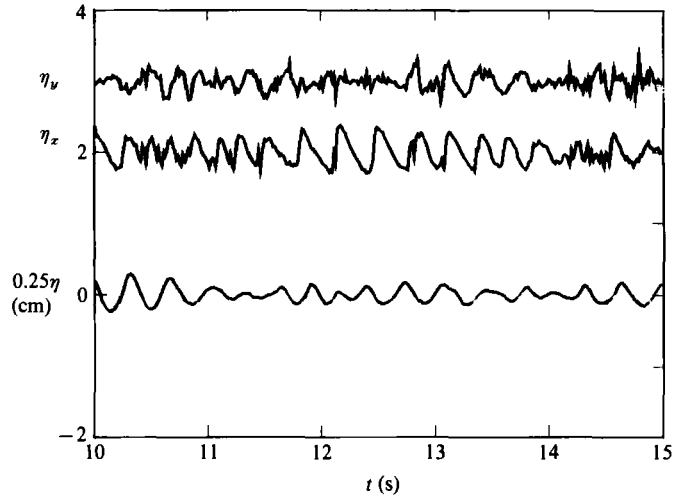

FIGURE 2. Time series of surface displacement (η), downwind slope (η_x) and crosswind slope (η_y). (η_x and η_y are offset by 2 and 3 units, respectively.) The wind speed is 4 m s^{-1}. No mechanical wave is present. (Reproduced from Miller & Shemdin 1991.)

end of the tank. The amplitude of the mechanical surface waves was kept constant at 4.1 cm and the fundamental period was 2 s. A wave absorber consisting of a transite asbestos cement surface with slope 1/12 for 3.5 m followed by a slope of 1/8 for 12.7 m was situated at the downwind end of the tank. The reflection coefficient of the fundamental 2 s wave was previously measured as about 0.1 and less than 0.05 for its harmonics. Time series of surface displacement were obtained using a capacitance wave gauge which responds to frequencies up to 8 Hz.

Crosswind and downwind components of the surface slope were measured at a fetch of 24.3 m using a laser slope sensor which measures the refraction of a light beam penetrating the air–water interface, as described by Tober, Anderson & Shemdin (1973) and Palm, Anderson & Reece (1977). Instruments of this type have been used by several authors (for example, Cox 1958; Long & Huang 1976; Hughes & Grant 1978; Tang & Shemdin 1983, Shemdin & Hwang 1988). Owing to the fast response of the optical system, rapid slope variations due to wave motion are easily detected. The shortest wave that can be detected is determined by the spot size of the laser beam, which is less than 3 mm in diameter. By positioning the laser slope sensor close to the capacitance wave gauge, and obtaining simultaneous measurements from the two instruments, changes in the short-wave slopes due to the passage of the long waves could be detected. However, the 'fish line' effect due to the passage of water past the wave gauge, was negligibly small.

3. Modulation of slope variance

Part of a time series of the surface displacement, η, of wind waves in the absence of a mechanical wave, as measured by the capacitance wave gauge, is plotted in figure 2. The dominant wave has a period of about 0.3 s at a wind speed of 4 m s^{-1}. The downwind and crosswind components of surface slope, η_x and η_y respectively, are also shown. Figure 3 shows the wind waves superimposed on the mechanically generated 2 s waves.

The variation of the statistics of wind waves at different phases of the current was found by averaging over equal phases of the mechanical wave. The period, T, and

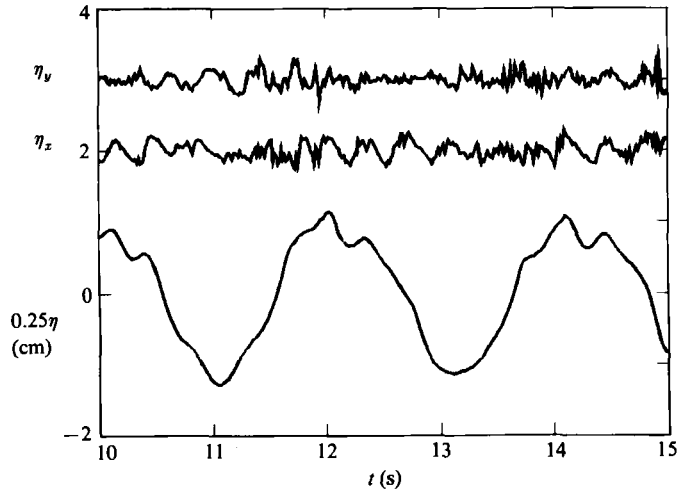

FIGURE 3. As for figure 2, but with 2 s mechanical wave present. (Reproduced from Miller & Shemdin 1991.)

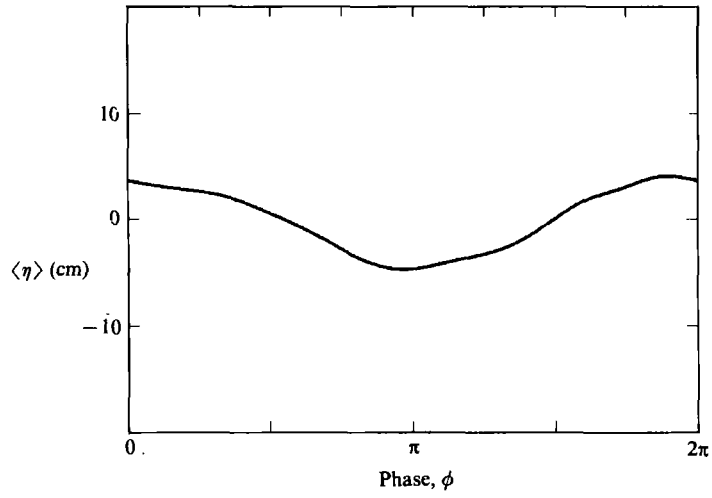

FIGURE 4. Surface displacement averaged over 75 periods, showing the 2 s mechanical wave. (Reproduced from Miller & Shemdin 1991.)

phase, ϕ, of the latter, were determined by maximizing the coherence of the surface displacement with a cosine of variable period, 2.0 ± 0.2 s, and variable phase. Figure 4 shows $\langle\eta\rangle$, the surface displacement, averaged over 75 periods. (Phase-averaged quantities are denoted using angle brackets.) The phase is defined by $\phi = 2\pi t/T$, with time, t, measured from the crest of $\langle\eta\rangle$. The wave paddle does not generate a purely sinusoidal disturbance, as is apparent in figure 5, which shows $\langle\eta_x\rangle$, the phase-averaged downwind component of the slope. Fourier analysis reveals components at the fundamental frequency,

$$\Omega_1 = 2\pi/T, \tag{1}$$

and at its harmonics,

$$\Omega_n = n\Omega_1. \tag{2}$$

The latter give only a small contribution to the surface displacement, but are significant in the downwind slope, which has contributions from up to the sixth harmonic (see table 1).

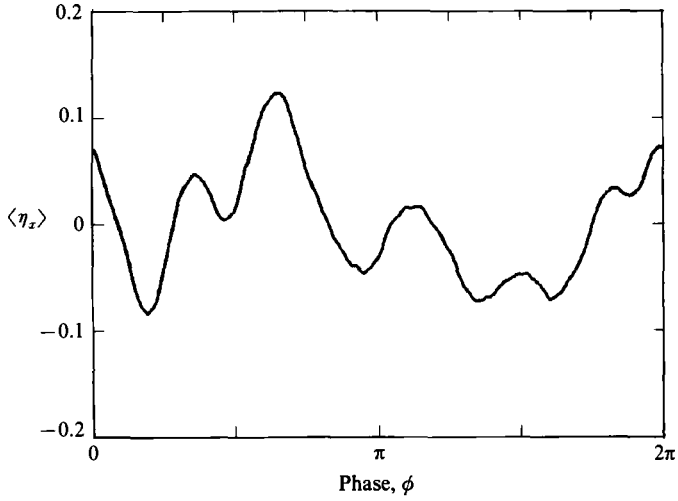

FIGURE 5. Downwind component of surface slope averaged over 75 periods. Significant amounts of the second and third harmonics of the fundamental oscillation are present. The wind speed is 1.5 m s^{-1}.

n	A_n (cm)	$K_n A_n$
1	4.11	0.043
2	0.40	0.015
3	0.46	0.038
4	0.08	0.013
5	0.01	0.008
6	0.02	0.003

TABLE 1. Fourier amplitudes of surface displacement, A_n, and downwind slope, $K_n A_n$, measured independently when no wind was blowing

$\langle \eta \rangle$ is modelled by

$$\langle \eta \rangle = \sum_{n=1}^{N} A_n \cos(\Omega_n t + \phi_n), \tag{3}$$

where the amplitudes A_n and phases ϕ_n were obtained numerically from Fourier decomposition of $\langle \eta \rangle$. Table 1 shows the Fourier amplitudes of surface displacement, A_n, measured with the capacitance wave gauge, together with the Fourier components of downwind slope, $K_n A_n$, measured independently with the laser slope gauge. Figure 6 shows K_n, the wavenumber of harmonic n, versus frequency Ω_n deduced from the ratio of $K_n A_n$ to A_n. The result is consistent with the dispersion relation for free surface waves,

$$\Omega_n^2 = g K_n \tanh(K_n d), \tag{4}$$

where g is acceleration due to gravity and d is the mean water depth. This result is expected for waves produced by a paddle wave generator of the type used here. It is noted that since the harmonics are coupled to the wave maker and have period T/n, the resultant disturbance at the instrument location due to the wave maker is periodic in time with period T.

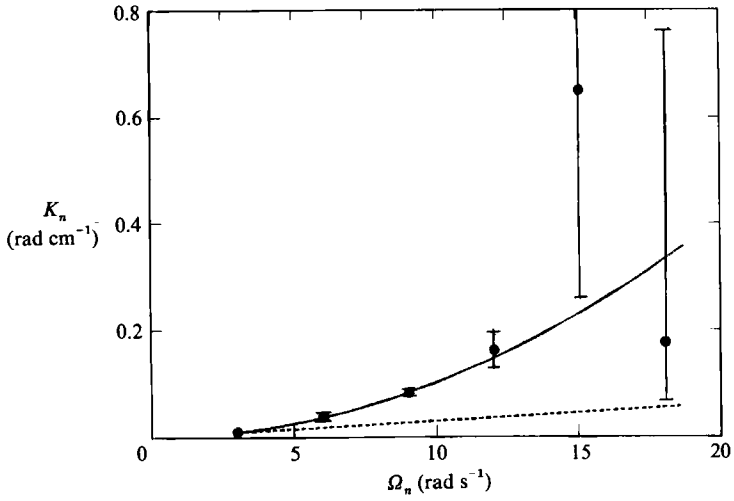

FIGURE 6. Dispersion relation of the waves produced by the paddle wave generator (solid circles), derived from the phase-averaged surface displacement and slope. The error bars show plus and minus one standard deviation of the estimate of K_n. Also shown are the dispersion relations of free gravity waves (solid line) and of waves bound to the fundamental oscillation (dashed line).

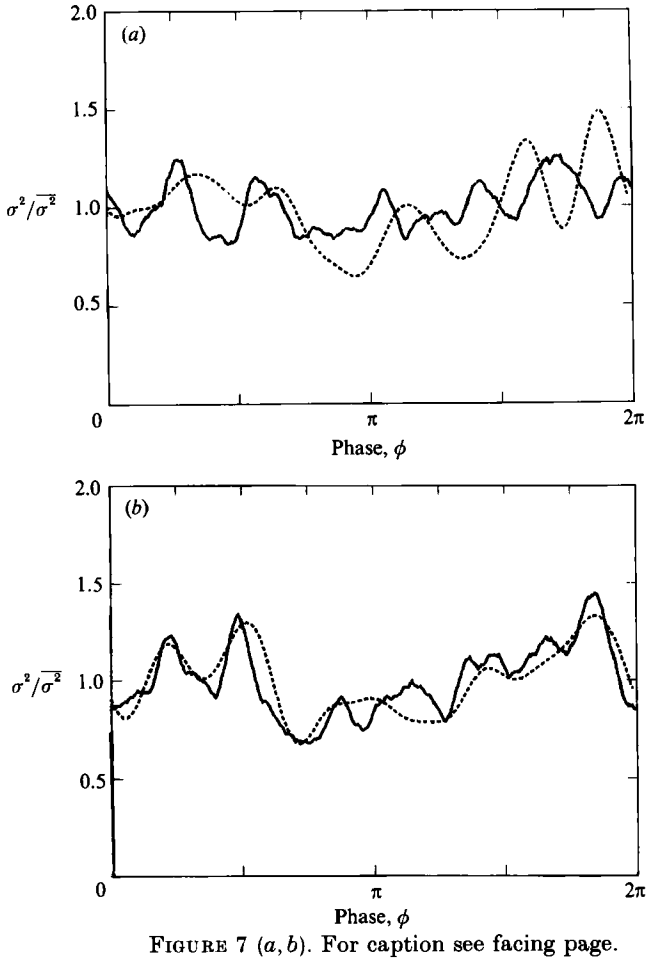

FIGURE 7 (*a*, *b*). For caption see facing page.

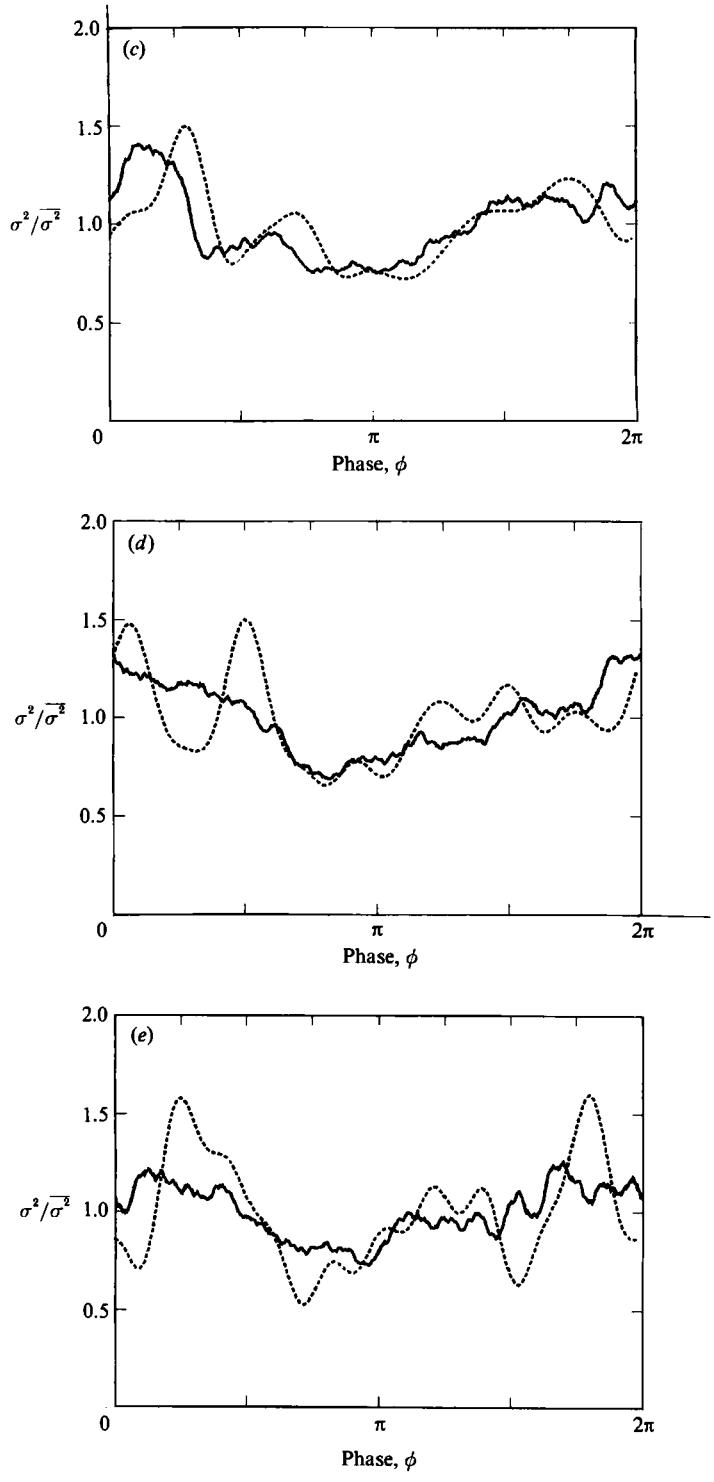

FIGURE 7. Variance of surface slope, normalized by its average value over a long-wave period. Data are shown by a solid line and the dashed line is the theoretical result of Longuet-Higgins & Stewart (1960), computed using 10 Fourier components. The wind speeds are (*a*) 1.5 m s^{-1}, (*b*) 4 m s^{-1}, (*c*) 6.5 m s^{-1}, (*d*) 9 m s^{-1} and (*e*) 10 m s^{-1}.

Wind speed W (m s^{-1})	Short-wave age, c/W	Long-wave age, C_1/W	$\overline{\sigma^2}$ (without long wave)	$\overline{\sigma^2}$ (with long wave)
1.5	0.19	2.00	0.002	0.022
4.0	0.13	0.75	0.038	0.026
6.5	0.10	0.46	0.056	0.045
9.0	0.09	0.33	0.063	0.055
10.0	0.08	0.30	0.063	0.059

TABLE 2. Variance of short-wave slope averaged over the long-wave period. c and C_1 denote the phase speeds of the dominant short and long waves, respectively

The variance of the short surface slopes at different phases of the long wave, was examined by calculating

$$\sigma^2 = \langle(\eta_x - \langle\eta_x\rangle)^2\rangle + \langle(\eta_y - \langle\eta_y\rangle)^2\rangle. \tag{5}$$

In figure 7 $\sigma^2/\overline{\sigma^2}$ is plotted as a function of ϕ at the five wind speeds, W (full line). Here $\overline{\sigma^2}$ is the mean value of σ^2 over the wave period T, and is tabulated in table 2 as a function of wind speed. For comparison, the value of $\overline{\sigma^2}$ obtained when no modulating wave was present is also tabulated. We note that, for $W \geqslant 4.0$ m s^{-1}, the presence of the long wave reduces $\overline{\sigma^2}$, the greatest reduction being at low wind speeds. The reduction of the wave amplitude of short waves on long waves has been reported by Mitsuyasu (1966), Phillips & Banner (1974), and Donelan (1987). Phillips & Banner (1974) showed that the orbital velocity of the long wave causes the surface drift velocity to vary with phase of the long wave. They proposed that this would result in enhanced breaking at the long-wave crests, leading to a reduction in the r.m.s. height of the short waves. Plant & Wright (1977), however, argued that the role of the wind drift current in limiting the short-wave amplitude was small.

The very low value of $\overline{\sigma^2}$ at 1.5 m s^{-1} is thought to be evidence of a surface slick. The minimum surface friction speed required for wave generation for a clean surface has been estimated by Miles (1962) and van Gastel, Janssen & Komen (1985) as about 5 cm s^{-1}. Assuming that in a wave tank the friction speed is given by $0.05W$ (Gottifredi & Jameson 1970; Plant & Wright 1977) this corresponds to a wind speed of $W \approx 1.0$ m s^{-1}. When a film is present, Miles estimated that this minimum is increased to about 17.5 cm s^{-1}, whereas Gottifredi & Jameson found that it could increase up to 20 cm s^{-1}, corresponding to $W \approx 4.0$ m s^{-1}. Evidently, the mean surface drift introduced by the deterministic wave disrupted the surface film, and wind waves could then be generated at the lowest wind speed.

4. Comparison with the theory of Longuet-Higgins & Stewart (1960)

Longuet-Higgins & Stewart (1960) considered the changes in a group of short gravity waves riding on a longer surface wave, $A_1 \cos(\Omega_1 t + \phi_1)$, of small slope, $K_1 A_1$. They showed that, in the absence of external sources and nonlinear effects such as wave breaking, the energy, E, of the short waves is governed by

$$\frac{\partial E}{\partial t} = \frac{\partial}{\partial x}[E(c_g + U) + S_x U], \tag{6}$$

where c_g and S_x are the group velocity and radiation stress of the short waves,

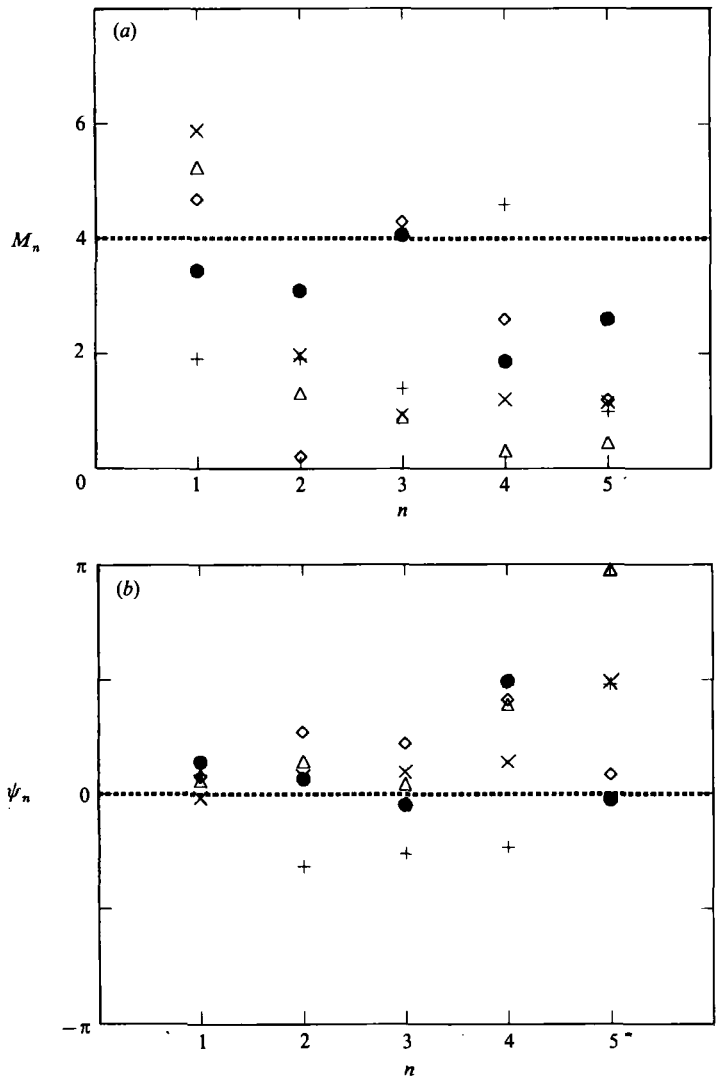

FIGURE 8. (*a*) Amplitude and (*b*) phase of the Fourier components of the modulation transfer function, defined by (9), at wind speeds 1.5 m s^{-1} (+), 4 m s^{-1} (●), 6.5 m s^{-1} (◇), 9 m s^{-1} (×) and 10 m s^{-1} (△).

respectively, and U is the current due to the orbital motions of the long wave. Generalizing their solution of (6) to a spectrum of non-interacting gravity waves travelling on a long wave with displacement given by (3), gives

$$\sigma^2(\phi) = \overline{\sigma^2}\left[1 + \sum_{n=1}^{N} (\tfrac{1}{2}\coth(K_n d) + \tfrac{1}{2}\tanh(K_n d)) K_n A_n \cos(\Omega_n t + \phi_n)\right]. \tag{7}$$

To compare this with the data, $\sigma^2(\phi)$, equation (7), was computed using K_n calculated from (4), and A_n obtained from the Fourier decomposition of $\langle\eta\rangle$ at each wind speed. The results are shown as dashed lines in figure 7.

A more detailed comparison is obtained by inspecting the complex Fourier

amplitudes of the linear modulation transfer function (MTF); if σ^2 is decomposed into

$$\sigma^2(\phi) = \overline{\sigma^2}\left[1 + \sum_{n=1}^{N} B_n \cos(\Omega_n t + \theta_n)\right], \tag{8}$$

the amplitude, M_n, and phase, ψ_n, of the nth component of the MTF are defined by

$$M_n = \frac{B_n}{K_n A_n}, \quad \psi_n = \theta_n - \phi_n. \tag{9}$$

A positive value of ψ_n indicates that modulation of σ^2 at frequency Ω_n lags that component of modulating current, that is, the modulation occurs at a later time. The first five components of the modulation are plotted in figure 8.

For the conditions of this experiment, the deep-water condition, $K_n d \geqslant 1.5$, is satisfied for all n. The MTF predicted by (7) therefore has $\psi_n = 0$ with $M_n \approx 4$ for all n, the levels being indicated by dashed lines in figure 8.

The goodness of fit of (7) to the data is clearly a function of wind speed, the best agreement being obtained at the intermediate values, 4 and 6.5 m s^{-1}, since in these cases M_n is close to 4. (The low value of M_2 at 6.5 m s^{-1} is not significant since $\langle\eta\rangle$ and σ^2 have only small contributions from the first harmonic.) The phase agreement at 4 m s^{-1} is also excellent, but at 6.5 m s^{-1} harmonics $n = 2$, 3 and 4 in σ^2 lead those in $\langle\eta\rangle$ by about 45°, as is apparent in figure 7(*c*). At the lowest wind speed, 1.5 m s^{-1}, the agreement between data and theory is poor, the modulation in the data being too small at low frequencies. Also, in this case the harmonics in σ^2 lag those in $\langle\eta\rangle$ by 45°. At the highest speeds, 9 and 10 m s^{-1}, modulation at the fundamental frequency is somewhat amplified compared to the intermediate wind speed cases, while it is reduced in the harmonics. The phase agreement is, however, quite good.

5. Discussion

Equation (6) was formulated for short gravity waves isolated from external effects such as wind input, and for which nonlinear interactions and wave breaking are not important. Its applicability to the conditions of the present experiment are examined as follows.

The importance of energy input from wind to a wave group of dominant frequency, f_p, can be estimated by evaluating the ratio of the wind growth rate, β, to the long-wave frequency, Ω_1. In this experiment $\Omega_1 \approx 3$ rad s^{-1}. When β is much less than Ω_1 the characteristic timescale of growth due to wind, β^{-1}, is long compared with the wave period, so that wind growth can be neglected. In this case (6) might be expected to describe the modulation of the variance of surface slopes. However, when β/Ω_1 is not small, the effect of wind input in the modulation process must be considered. Table 3 shows the growth rate, $\beta(f_p)$, evaluated using Plant's (1982) form with the friction speed evaluated as $0.05W$,

$$\beta = 6.3 \times 10^{-4}(W/c)^2 f_p, \tag{10}$$

where c is the phase speed at frequency f_p.

As the wind speed increases, the wind wave spectrum becomes broader as the energy of the small waves increases. The slope frequency spectra of the short waves, $S(f)$, where

$$\overline{\sigma^2} = \int_0^\infty S(f)\,\mathrm{d}f, \tag{11}$$

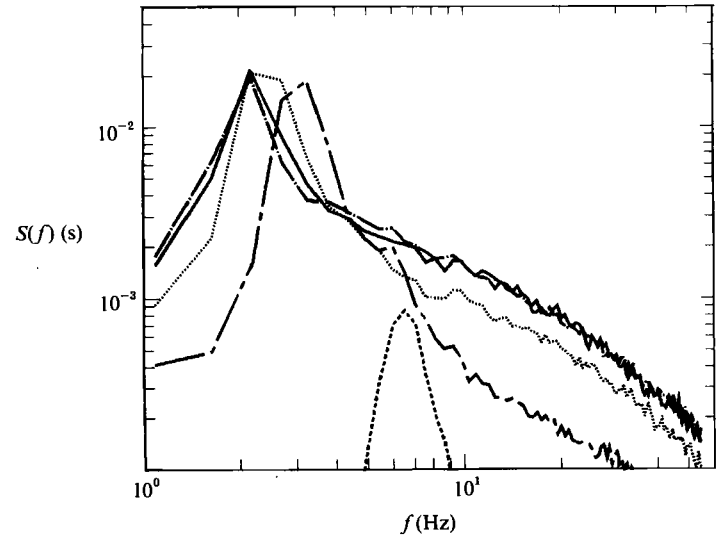

FIGURE 9. Slope frequency spectra at wind speeds 1.5 m s^{-1} (– – –), 4 m s^{-1} (——), 6.5 m s^{-1} (·····), 9 m s^{-1} (——), and 10 m s^{-1} (—·—·). No mechanical wave is present. (Reproduced from Miller & Shemdin 1991.)

W (m s^{-1})	f_p (Hz)	$\beta(f_p)$ (s^{-1})	f_{med} (Hz)	$\beta(f_{med})$ (s^{-1})	$\dfrac{\beta(f_{med})}{4\Omega_1 K_1 A_1}$
1.5	6.0	0.09	6.0	0.09	0.19
4.0	3.0	0.14	3.0	0.14	0.28
6.5	2.5	0.17	4.0	0.69	1.37
9.0	2.0	0.17	10.0	9.61	19.18
10.0	2.0	0.20	10.0	11.87	23.69

TABLE 3. Growth rate due to the wind

are plotted in figure 9. At 4 m s^{-1} 70% of the total area lies below 5 Hz, compared with only 40% at 9 m s^{-1}. A possibly more accurate estimation of the growth rate may be obtained, therefore, by evaluating β at, for example, the median frequency, f_{med}, of the slope spectrum, where

$$\int_0^{f_{med}} S(f)\,df = \tfrac{1}{2}\overline{\sigma^2}. \tag{12}$$

The results, which except for the lowest wind speed were obtained when no mechanical wave was present, are shown as $\beta(f_{med})$ in table 3. At 9 and 10 m s^{-1}, $\beta(f_{med})/\Omega_1 \geqslant 3$ suggesting that wind generation effects must be significant in those cases.

The relative importance of the energy input by the wind to the modulation of the short waves by the orbital straining of the long waves, can be estimated by considering the ratio of β/Ω_n to $4K_nA_n$. With β evaluated at f_{med}, this is shown in table 3 for the fundamental frequency of the long wave. Interestingly, $\beta/(4\Omega_1 K_1 A_1)$ is much greater than unity for the two highest wind speeds.

The steepness of the short waves increases with wind speed so that the nonlinear effects of wave breaking and wave–wave interactions are expected to become

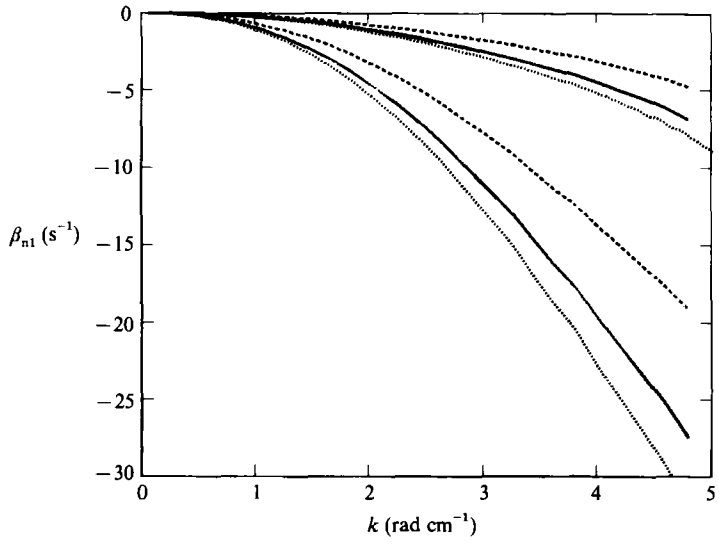

FIGURE 10. Nonlinear transfer for three-wave interactions for wind speeds 4 and 9 m s^{-1} and $D(\theta, k) = a_p \cos^p(\frac{1}{2}\theta)$ with $p = 2$ (– – –), 6 (——) and 10 (·····).

W (m s^{-1})	k_{med} (rad cm^{-1})	$\beta_{nl}(k_{med})$ (s^{-1})	$\dfrac{\beta_{nl}(k_{med})}{\Omega_1}$	$\dfrac{\beta_{nl}(k_{med})}{4\Omega_1 K_1 A_1}$
4.0	0.16	0.00	0.00	0.00
6.5	0.64	0.13	0.04	0.26
9.0	2.60	7.45	2.38	14.87
10.0	2.60	7.45	2.38	14.87

TABLE 4. Nonlinear transfer rate due to three-wave interactions

increasingly significant. The weakly nonlinear wave–wave interactions are of third order in the wave slope for short gravity waves, and second order for capillary–gravity waves. The rate of energy transfer due to the latter, β_{nl}, was computed using the expression derived by Valenzuela & Laing (1972). The results evaluated at $k = k_{med}$, where

$$2\pi f_{med} = \left(gk_{med} + \frac{\tau}{\rho}k_{med}^3\right)^{\frac{1}{2}} \tag{13}$$

(τ and ρ are the surface tension and density of water), are given in table 4 for the four highest wind speeds (the lowest wind speed case was not computed). Details of the wavenumber spectrum used in the calculation are given in the Appendix.

Comparison of tables 3 and 4 shows that the estimates of β_{nl} are similar to those obtained for the growth rate due to the wind, with a sharp distinction between $W \leqslant 6.5$ m s^{-1}, where the transfer rate is small compared with the long-wave frequency and energy transfer is a minor effect in comparison with orbital straining, and $W \geqslant 9$ m s^{-1}, where the three-wave interactions play an important role.

The wind drift current, u_d, has not been considered in the above calculations. For short waves at high wind speeds the wind drift current can be of the same magnitude as the intrinsic phase speed of short gravity waves. For example, at a wind speed of 10 m s^{-1}, calculating the drift current as 3% of the wind speed, gives $u_d = 30$ cm s^{-1},

which is equal to the phase speed of a 5 cm wave in still water. If β is evaluated using (10) with c in the denominator calculated as the advected phase speed, the value of β will be reduced by a factor of about 4 at $W = 9$ m s^{-1} and 10 m s^{-1}, and by a smaller factor at the lower wind speeds. Also, if (13) is modified to include the wind drift, k_{med} will be reduced by a factor of about 2 at the highest wind speeds so that, from figure 10, β_{nl} is reduced by factor of about 4 in these cases. The distinction between the low and high wind cases in the relative importance of orbital straining and energy input from the wind or energy transfer due to three wave interactions, would be less dramatic than estimated above, but the trend is unchanged.

We note that at the highest wind speeds, (7) should be modified to include capillary–gravity waves, which make a significant contribution to $\overline{\sigma^2}$. If this is done, the theoretical MTF due to the orbital motions of the long wave becomes somewhat smaller than the value 4 found above for a spectrum of pure gravity waves. However, the application of a simple two-scale model to these very short waves is probably not realistic.

6. Conclusions

The most striking conclusion to be drawn from these measurements is that the modulation of the short waves is determined not by the long-wave amplitude, A_n, but rather the long-wave steepness, $K_n A_n$. Hence, the apparent phase and amplitude of the modulation may be related to wave components that are invisible to the eye.

More generally, the modulation of the short waves will be determined not by the *elevation* spectrum of the long waves but by the *slope* spectrum, as is emphasized by Longuet-Higgins (1991).

We have found that the modulation transfer function of the short waves is in agreement with the linearized, non-dissipative theory of Longuet-Higgins & Stewart (1960) only where that would be expected, namely when the short waves are not too steep, and the rate of growth due to the wind is relatively small. (We found poor agreement at the lowest wind speed, however.) With steeper short waves, we may expect two additional effects: strong short-wave interactions due to breaking, and weak non-dissipative short-wave interactions. For short capillary–gravity waves they are of second order (Valenzuela & Laing 1972), and for short gravity waves they are of third order (Hasselmann 1962). Their relative importance will vary with short-wave steepness.

Finally we remark that since the tangential wind stress is in part mediated by the short wind waves, our findings will have implications for the effect of swell on the mean wind stress, and on the modulation of the wind stress by the longer waves.

Paul Hwang and Dave Hayt were responsible for the data collection and the initial data processing was done by Paul Hwang. The authors appreciate their cooperation during the period of the above work. The work reported here was supported by the Office of Naval Research under the SAR Accelerated Research Initiative Program.

Appendix. Calculation of β_{nl}, the capillary–gravity wave–wave interaction rate

The spectrum of wave heights,

$$\langle \eta^2 \rangle = \int_0^\infty \int_{-\pi}^{\pi} \Psi(k, \theta)\, k \, \mathrm{d}k \, \mathrm{d}\theta, \tag{A 1}$$

W (m s^{-1})	k_p (rad cm^{-1})	Γ
4.0	0.16	56
6.5	0.25	21
9.0	0.36	13
10.0	0.36	13

TABLE 5

was modelled using the separable form

$$\Psi(k,\theta) = F(k)\,D(\theta,k), \tag{A 2}$$

where

$$\int_{-\pi}^{\pi} D(\theta,k)\,\mathrm{d}\theta = 1. \tag{A 3}$$

The directional spread function $D(\theta,k)$ was modelled by

$$D(\theta,k) = a_p \cos^p(\tfrac{1}{2}\theta), \quad p = p(k), \tag{A 4}$$

where the downwind direction is taken as $\theta = 0$.

The model used here is derived from consideration of the two components of the frequency slope spectrum obtained before the long wave was generated. Taking the minimum wind speed required for wave generation, as $W_{\min} = 2.7$ m s^{-1}, $F(k)$ is modelled, for 4 m s^{-1} $\leqslant W \leqslant$ 9 m s^{-1}, by (Shemdin & Miller 1991)

$$F(k) = 5\times10^{-4}(W-W_{\min})\frac{k^{-3.5}}{(g+\tau k^2/\rho)}\exp\left(-1.75\left(\frac{k_p}{k}\right)^2\right)\Gamma^M \quad \text{for} \quad k < k_\nu. \tag{A 5}$$

Here, g is gravitational acceleration, and ρ and τ are the density and surface tension of water. $k_\nu = 8$ rad cm^{-1} is the viscous cutoff, and

$$M = \exp\left(-\frac{(k^{\frac{1}{2}}-k_p^{\frac{1}{2}})^2}{0.32k_p}\right), \tag{A 6}$$

where $k_p = (2\pi f_p)^2/g$ is the peak wavenumber, and Γ and $M(k)$ define the height and shape of the spectral peak. Γ and k_p are wind-speed dependent as shown in table 5.

The part of the spectrum where viscosity is important is modelled by (Shemdin & Miller 1991)

$$F(k) = 4.8\times10^{-4}(W-W_{\min})\,k^{-5.5} \quad \text{for} \quad k > k_\nu. \tag{A 7}$$

Above $W = 9$ m s^{-1}, the frequency spectrum was found to saturate, so at 10 m s^{-1} $F(k)$ was modelled by the same form as at 9 m s^{-1}.

The nonlinear transfer due to three-wave interactions between gravity and capillary–gravity waves, $\partial\Psi/\partial t$, was calculated numerically using the expression given by Valenzuela & Laing (1972). The transfer rate, $\beta_{nl} \equiv -(1/\Psi)(\partial\Psi/\partial t)$, was also calculated for spread functions, $D(\theta,k)$, with $p = 2$, 6 and 10 for all k. The results are shown in figure 10 for $k \leqslant 5$ rad cm^{-1} and for wind speeds 4 and 9 m s^{-1}. The plots show that, as expected, the energy transfer is small for small wavenumbers and increases with wind speed. The fact that the transfer is largest for wave triads that are inclined at small angles, is reflected in β_{nl} increasing with p.

At wavenumbers beyond the peak of the spectrum, the angular spread increases so that the ratio of the crosswind and downwind components of the slope spectrum

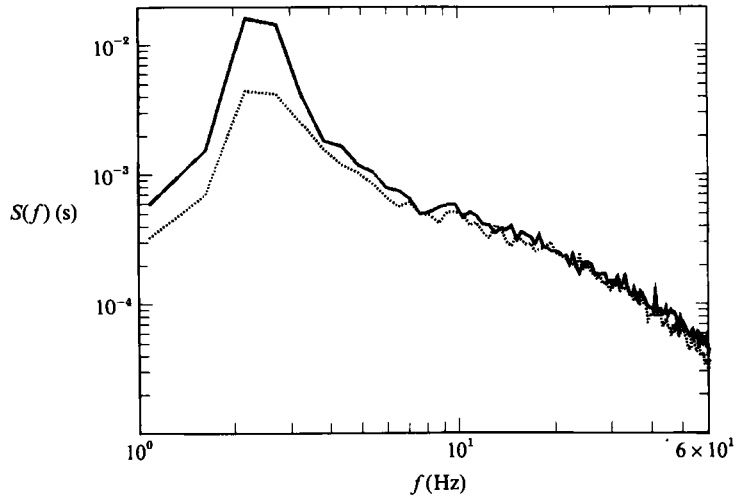

FIGURE 11. Downwind (——) and crosswind (·····) components of the slope frequency spectrum at wind speed 6.5 m s^{-1}, measured before the mechanical wave was generated. (Reproduced from Miller & Shemdin 1991.)

increases, as can be seen in figure 11. The model used here is $p = 10$ for $k \leqslant k_p$, $p = 2$ for $k > (g\tau/\rho)^{\frac{1}{2}}$ and decreasing linearly with k between the two limits. This model of the angular spreading function gives ratios of the crosswind to downwind slope spectrum which are in agreement with our observations. The resulting transfer rate is given in table 4.

REFERENCES

COX, C. S. 1958 Measurements of slopes of high frequency wind waves. *J. Mar. Res.* **16**, 199–225.

DONELAN, M. A. 1987 The effect of swell on the growth of wind waves. *Johns Hopkins Univ. APL Tech. Dig.* **8**, 18–23.

GASTEL, K. VAN, JANSSEN, P. A. E. M. & KOMEN, G. J. 1985 On phase velocity and growth rate of wind induced gravity-capillary waves. *J. Fluid Mech.* **161**, 199–216.

GOTTIFREDI, J. C. & JAMESON, G. J. 1970 The growth of short waves on liquid surfaces under the action of wind. *Proc. R. Soc. Lond.* A **319**, 373–397.

HASSELMANN, K. 1962 On the non-linear energy transfer in a gravity wave spectrum. *J. Fluid Mech.* **12**, 481–500.

HUGHES, B. A. & GRANT, H. L. 1978 The effect of internal waves on surface wind waves 1. Experimental measurements. *J. Geophys. Res.* **83**, 443–454.

KWOH, D. S. W., LAKE, B. M. & RUNGALDIER, H. 1988 Microwave scattering from internal wave modulated surface waves: A shipboard real aperture coherent radar study in the Georgia Strait experiment. *J. Geophys. Res.* **93**, 12235–12248.

LEWIS, J. E., LAKE, B. M. & KO, D. R. S. 1974 On the interaction of internal waves and surface gravity waves. *J. Fluid Mech.* **63**, 773–800.

LONG, R. B. & HUANG, N. E. 1976 On the variation and growth of wave-slope spectra in the capillary-gravity range with increasing wind. *J. Fluid Mech.* **77**, 209–228.

LONGUET-HIGGINS, M. S. 1987 The propagation of short surface waves on longer gravity waves. *J. Fluid Mech.* **177**, 293–306.

LONGUET-HIGGINS, M. S. 1991 A stochastic model of sea-surface roughness II., *Proc. Roy. Soc. Lond.* A, in press.

LONGUET-HIGGINS, M. S. & STEWART, R. W. 1960 Changes in form of short gravity waves on long waves and tidal currents, *J. Fluid Mech.* **8**, 565–583.

MILES, J. W. 1962 On the generation of surface waves by shear flows. *J. Fluid Mech.* **13**, 433–448.

MILLER, S. J. & SHEMDIN, O. H. 1991 Measurement of the hydrodynamic modulation of centimetre waves. *J. Geophys. Res.* **96**, 2749–2759.

MITSUYASU, H. 1966 Interactions between water waves and wind, 1. *Rep. Res. Inst. Appl. Mech. Kyushu Univ.* **14**, 67–88.

PALM, C. S., ANDERSON, R. C. & REECE, A. M. 1977 Laser probe for measuring 2D wave slope spectra of ocean capillary waves. *Appl. Opt.* **16**, 1074–1081.

PHILLIPS, O. M. & BANNER, M. L. 1974 Wave breaking in the presence of wind drift and swell. *J. Fluid Mech.* **66**, 625–640.

PLANT, W. J. 1982 A relationship between wind stress and wave slope. *J. Geophys. Res.* **87**, 1961–1967.

PLANT, W. J. & WRIGHT, J. W. 1977 Growth and equilibrium of short gravity waves in a wind-wave tank. *J. Fluid Mech.* **82**, 767–793.

REECE, A. M. 1978 Modulation of short waves by long waves. *Boundary-Layer Met.* **13**, 203–214.

SHEMDIN, O. H. & HWANG, P. A. 1988 Comparison of measured and predicted sea surface spectra of short waves. *J. Geophys. Res.* **93**, 13883–13890.

SHEMDIN, O. H. & MILLER, S. J. 1991 A model for the wave number spectrum of wind generated waves. (submitted).

TANG, S. & SHEMDIN, O. H. 1983 Measurement of high frequency waves using a weave follower. *J. Geophys. Res.* **88**, 9832–9840.

TOBER, G., ANDERSON, R. C. & SHEMDIN, O. H. 1973 Laser instruments for detecting water ripple slopes. *Appl. Opt.* **12**, 788–794.

VALENZUELA, G. R. & LAING, M. B. 1972 Nonlinear energy transfer in a gravity-capillary wave spectra, with applications. *J. Fluid Mech.* **54**, 507–520.

WRIGHT, J. A., PLANT, W. J., KELLER, W. C. & JONES, W. L. 1980 Ocean wave-radar modulation transfer functions from the west coast experiment. *J. Geophys. Res.* **85**, 4957–4966.